Local density of states in mesoscopic samples from scanning gate microscopy

M. G. Pala,[1] B. Hackens,[2] F. Martins,[3] H. Sellier,[3] V. Bayot,[2] S. Huant,[3] and T. Ouisse[3]
[1]*IMEP-LAHC-MINATEC (UMR CNRS/INPG/UJF 5130), Boîte Postale 257, 38016 Grenoble, France*
[2]*CERMIN, DICE Laboratory, UCL, B-1348 Louvain-la-Neuve, Belgium*
[3]*Institut Néel, CNRS, and Université Joseph Fourier, Boîte Postale 166, 38042 Grenoble, France*
(Received 8 November 2007; revised manuscript received 29 January 2008; published 10 March 2008)

We study the relationship between the local density of states (LDOS) and the conductance variation ΔG in scanning-gate-microscopy experiments on mesoscopic structures as a charged tip scans above the sample surface. We present an analytical model showing that in the linear-response regime the conductance shift ΔG is proportional to the Hilbert transform of the LDOS and hence a generalized Kramers–Kronig relation holds between LDOS and ΔG. We analyze the physical conditions for the validity of this relationship both for one-dimensional and two-dimensional systems when several channels contribute to the transport. We focus on realistic Aharonov–Bohm rings including a random distribution of impurities and analyze the LDOS-ΔG correspondence by means of exact numerical simulations, when localized states or semiclassical orbits characterize the wave function of the system.

DOI: 10.1103/PhysRevB.77.125310 PACS number(s): 73.21.La, 73.23.Ad, 03.65.Yz, 85.35.Ds

I. INTRODUCTION

Scanning probe microscopy (SPM) is nowadays an essential technique to measure local electronic properties of mesoscopic structures. Scanning tunnel microscopy (STM), consisting in probing the sample surface with a metallic tip, is the most popular among all SPM techniques. STM experiments have first enabled the detection of standing wave pattern in confined surface electron systems such as quantum corrals.[1] The physical interpretation of such images is straightforward since they are derived from direct tunneling between the surface electrons and the tip. Hence, STM images represent the density of states of the system at a given position of the scanning probe.[1]

Later on, another SPM technique, named scanning gate microscopy (SGM), has been introduced in order to obtain similar information for structures buried under an insulating layer. This technique consists in scanning a biased tip over the sample surface. The gate acts as a local electrostatic (repulsive or attractive) potential on the electronic system and allows us to obtain two-dimensional (2D) conductance (or resistance) images of the scanned area as a function of the tip position. At the present time, SGM or an alternative technique called scanning capacitance microscopy has been adopted to investigate the physics of quantum points contacts,[2–6] quantum dots,[7,8] carbon nanotubes,[9] open billiards,[10] and edge states in the integer quantum Hall regime.[11–14] SGM on InAs nanowires has evidenced the presence of multiple quantum dots inside the structure corresponding to circular Coulomb blockade peaks in the conductance plots.[15]

From a theoretical point of view, numerical simulations based on the Keldysh–Green functions formalism have been exploited to demonstrate wave function imaging in open quantum dots[16,17] and to associate conductance images to electron flow in quantum point contacts.[18,19]

Recently, isophase lines for electrons in an electrostatic Aharonov–Bohm (AB) experiment[20] and local-density-of-states (LDOS) mapping inside a coherent AB ring[21] have been reported. In the latter work, both experimental curves and numerical simulations have found a linear dependence of the conductance variation on the tip voltage. Interestingly, clear wave function images were obtained only in this case,[21] suggesting to limit the imaging technique to the linear-response regime. It was also noticed that the simulated conductance maps were not significantly influenced by the particular shape adopted to mimic the effective perturbing potential due to the scanning gate.

Since SGM is essentially an indirect measurement of the 2D electron gas (2DEG) properties, a physical interpretation of conductance images is not immediate. Therefore, in this paper, we try to clarify the physical meaning of SGM experiments and to isolate the experimental conditions under which the linear response-regime holds.

In Sec. II, we present an analytical model which provides a simple physical interpretation of the SGM conductance images in the single-channel transmission regime. We find that the conductance correction due to the scanning tip is related to the Hilbert transform of the LDOS of the system. Moreover, we analyze the spatial and energetic conditions on the perturbing potential under which this direct relation is maintained.

In Sec. III, we present 2D numerical simulations of a realistic quantum ring characterized by the presence of randomly localized impurities. Our calculations are based on a recursive Green's functions method and illustrate the correspondence between LDOS and conductance images of the system in such a complex case. In particular, we address the interesting case for which the wave function of the system is dominated by localized states due to charged impurities or by recursive semiclassical orbits.

Section IV summarizes the relevant results.

II. SINGLE-CHANNEL TRANSMISSION

In this section, we evaluate the effect of a local perturbation on the total transmission of a noninteracting system connected to single-channel leads. We adopt the Landauer–

Büttiker transport theory assuming the zero-temperature limit.[22]

We consider a multistate system connected to one-dimensional leads and neglect the effect of inelastic scattering and electron-electron interactions. These assumptions are valid in the case of low-temperature experiments on mesoscopic samples working in the phase coherent transport regime.[23] We model our system as a chain of N sites with the ith on-site potential ϵ_i coupled to two semi-infinite reservoirs with fixed chemical potentials. The coupling strength with the left and the right reservoir is denoted by $\Gamma_{L,R}=2\pi|V_{L,R}|^2\rho_{L,R}$, where $V_{L,R}$ is the coupling with the leads and $\rho_{L,R}$ is the density of states of the reservoirs, respectively. Moreover, each site is coupled only to its nearest neighbor with coupling constant V, which for simplicity we assume to be position independent.

Since the linear conductance of a system with Fermi energy ϵ_F is determined by the propagator from site 1 to site N, we simply need to evaluate the element $G^R(x_N,x_1)=G^R_{N,1}$ of the retarded Green's function of the system G^R. By adopting the common assumption of a large bandwidth coupling with the reservoirs, the conductance G reads

$$G(\epsilon_F)=G_0\Gamma_L\Gamma_R|G^R_{N,1}(\epsilon_F)|^2, \tag{1}$$

where G_0 is the quantum of conductance.[24] Further, we will use the well known fact that the LDOS at x_i is proportional to the imaginary part of the diagonal elements of the retarded Green's function $G^R(x_i,x_i)=G^R_{i,i}$ as

$$\rho(x_i;\epsilon_F)=-\frac{1}{\pi}\,\mathrm{Im}[G^R_{i,i}(\epsilon_F)], \tag{2}$$

which derives from the pole structure of the Green's function.[25] In order to relate the conductance in Eq. (1) and the LDOS in Eq. (2), we exploit the Dyson equation,

$$G^R=g^R+g^R\hat{V}G^R=g^R+G^R\hat{V}g^R, \tag{3}$$

where g^R is the unperturbed Green's function of the isolated sites and $\hat{V}$ corresponds to the hopping connection between sites. From Eq. (3), one can obtain the relation between the propagator $G^R_{i+1,1}$ and $G^R_{i,i}$ or $G^R_{i+1,i+1}$ as[26]

$$G^R_{i+1,1}=G^R_{i+1,i+1}Vg^R_{i,i}=g^R_{i+1,i+1}VG^R_{i,i}. \tag{4}$$

Hence, by recursively applying Eq. (4) to express $G^R_{N,1}$ in terms of $G^R_{i,i}$, we can rewrite Eq. (1) as

$$G=G_0\Gamma_L\Gamma_R|V|^{2(N-1)}|G^R_{i,i}|^2\prod_{j\neq i}|g^R_{j,j}|^2, \tag{5}$$

where the index i can take any value between 1 and N. Further, since we are interested in studying the stationary regime of transport, it is convenient to write the Green's functions in the energy space representation by performing a Fourier transform. We have $g^R_{i,i}=[\epsilon_F-\epsilon_i+i0^+]^{-1}$ and $G^R_{i,i}=[(g^R_{i,i})^{-1}-\Sigma_i]^{-1}=[(g^R_{i,i})^{-1}-\Lambda_i+i\Gamma_i]^{-1}$, where 0^+ is a positive infinitesimal number and $\Sigma_i=(\Lambda_i-i\Gamma_i)$ is the self-energy including the interactions with the system on the local ith Green's function.[25]

We now consider the effect on the transmission of a local perturbing potential which can be physically associated with the action of a charged tip scanning the system. We mimic the effect of the charged tip at position x_i as a renormalization of the on-site energy $\epsilon_i+\Lambda_i\rightarrow\epsilon_i+\Lambda_i+U$, where U is the perturbing potential. Assuming that the potential strength is sufficiently "weak," the conductance correction is linear in U and reads

$$\frac{\Delta G}{G}(x_i;\epsilon_F)=2U\,\mathrm{Re}[G^R_{i,i}(\epsilon_F)]. \tag{6}$$

Notice that Eq. (6) can be expressed in terms of sensitivities[27] and hence connected to the scattering-matrix elements of the system.

By comparing Eq. (6) with Eq. (2), we find that the conductance variation due to the action of a local perturbing potential and the LDOS are related in the same way as the real and the imaginary part of the Green's function $G^R_{i,i}$, namely, by a Kramers–Kronig relation. Mathematically, this is expressed in terms of the Hilbert transform $\mathrm{Re}[G^R_{i,i}(\omega)]=\mathcal{H}\{\mathrm{Im}[G^R_{i,i}(\omega)]\}=-\frac{1}{\pi}\mathcal{P}\int d\omega'\frac{1}{\omega-\omega'}\,\mathrm{Im}[G^R_{i,i}(\omega')]$, where $\mathcal{P}$ stands for the Cauchy principal part. Therefore, in the linear-response regime, the conductance (transmission) correction is proportional to the Hilbert transform of the local density of states. Notice that the sign of the conductance correction is determined by both the perturbing potential U and by the relative position of the Fermi energy with respect to $\epsilon_i+\Lambda_i$.

The physical origin of such a relationship can be understood by noticing that the main effect of the local perturbing potential U is to renormalize the real part of the self-energy.

By analyzing Eq. (6), we can deduce the conditions of validity of the LDOS-ΔG correspondence. In order to deal with a weak perturbation giving rise to a linear correction, the condition $|U|<|\epsilon_F-\epsilon_i-\Lambda_i|$ has to hold. A condition on the extension of the perturbing potential is given by the spatial periodicity of the wave function and limits the spatial range of the effective potential below the half-Fermi wavelength $\lambda_F/2$. Nevertheless, notice that in the multichannel transmission case that we discuss in Sec. III, the spatial periodicity of the LDOS can be larger than $\lambda_F/2$.

Interestingly, in the single-channel transmission regime the LDOS is usually a sinusoidal function of the spatial coordinate, whereas the Hilbert transform of such a function alters the original function by only a $\pi/2$ phase shift. More precisely, the Hilbert transform adds a $+\pi/2$ phase for right-going states and $-\pi/2$ for left-going states. This justifies the use of a scanning local perturbation, like that obtained in SGM experiments, as an efficient tool to image the LDOS of the system.

We also notice that the Hilbert transform is the convolution of the LDOS with the inverse of the Fermi energy and can be interpreted as a filter for the states closest to the Fermi level. This is consistent with SGM experiments on QPCs[2] with several occupied modes, where conductance images are dominated by the contribution of the mode closest to the Fermi energy.

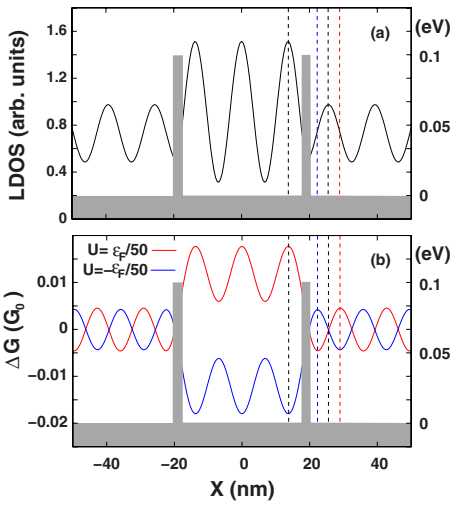

FIG. 1. (Color online) (a) LDOS and (b) conductance variation ΔG for a double-barrier system. The distance between the two barriers of height 0.1 eV is $L=18$ nm, the effective mass, is $m=0.04m_0$ with m_0 the free electron mass and the Fermi energy is $\epsilon_F=0.05$ eV. The perturbing potential used to obtain (b) is a square repulsive (red line) or attractive (blue line) barrier with height $U_0=\pm\epsilon_F/50$ and width $W=10$ nm. Dashed vertical lines indicate the maximum position of LDOS (black line) and ΔG (red or blue line).

A. Symmetric double barrier

In order to give a practical application of the model, we study the simple case of a symmetric double barrier. In Fig. 1, we show the LDOS of the unperturbed system and the conductance correction due to a scanning potential acting as a local scatterer. The conductance is computed by means of Eq. (1) after numerical calculation of the total Green's function. The local perturbing potential is assumed to be a rectangular-shaped barrier with height $U_0=\epsilon_F/50$ (or $U_0=-\epsilon_F/50$) and width $W=10$ nm smaller than $\lambda_F/2\sim 14$ nm.

Let us discuss the ΔG-LDOS correspondence separately for the two regions inside and outside the two barriers. We model the two barriers by using the same scattering matrix S which can be parametrized as

$$S=\begin{pmatrix} r & t \\ t & r \end{pmatrix}=\begin{pmatrix} e^{i\alpha}|r| & ie^{i\beta}|t| \\ ie^{-i\beta}|t| & e^{-i\alpha}|r| \end{pmatrix}, \tag{7}$$

where α and β are real phases ($\beta=0$ if time-reversal symmetry holds) and $|t|=\sqrt{T}$, $|r|=\sqrt{1-T}$, with T the transmission probability. In order to compute the LDOS inside the two barriers, we evaluate the wave function for left- and right-injected states by imposing the proper boundary conditions. We obtain $\Psi_L(x)\propto[e^{ik_F(x-L/2)}+|r|e^{i\alpha}e^{-ik_F(x-L/2)}]$ and $\Psi_R(x)\propto[e^{-ik_F(x+L/2)}+|r|e^{-i\alpha}e^{ik_F(x+L/2)}]$, with k_F the Fermi wave vector and L the distance between the two barriers. By estimating the LDOS of the system as the independent sum of left-injected and right-injected states, we obtain $\rho(x)\propto[1+|r|^2+2|r|\cos(k_FL)\cos(2k_Fx-\alpha)]$. The Hilbert transform of this function adds a $+\pi/2$ phase shift to the partial LDOS corresponding to the left-injected states and a $-\pi/2$ phase shift to the partial LDOS corresponding to the right-injected states. It reads $\mathcal{H}\{\rho(x)\}\propto[1+|r|^2+2|r|\cos(k_FL-\pi/2)\cos(2k_Fx-\alpha)]$ and it has the same spatial dependence as $\rho(x)$. An identical result is numerically recovered in Fig. 1 by computing the conductance variation due to a square perturbing potential. Notice that a further sign on the conductance variation can be determined by the choice of an attractive or repulsive potential.

The effect of the local scatterer is different in the spatial region outside the two barriers. On the left (right) of the barriers the LDOS shape is determined only by left (right)-injected states which gives $\rho(x)\propto\text{const}+\cos[2k_F(x\mp L/2)-\alpha]$. In fact, on the left (right) of the barrier, the right (left)-injected states contribute as a constant to the LDOS. The Hilbert transform of such a function gives the same expression with $a\pm\pi/2$ phase shift for right- and left-injected states. Again, this is the result found numerically in Fig. 1.

Finally, we address the case of the Fermi energy being equal to $\epsilon_i+\Lambda_i$. In this case, it turns out that $\text{Re}[G^R_{i,i})]=0$ and the system is "on-resonance." This condition gives a maximum of the transmission probability. In such a case, Eq. (6) vanishes and the correction to the transmission is given by the second order in U. It reads

$$\frac{\Delta G}{G}(x_i;\epsilon_F)=-\pi^2\rho^2(x_i;\epsilon_F)U^2. \tag{8}$$

Therefore, in the resonant case, the correction to the transmission is a monotonic function of the local density of states $\rho(x_i)$ and has a fixed sign.

B. Mesoscopic ring

We focus now on the simulation of an AB ring since such a structure is particularly suited to study phase coherence effects in mesoscopic physics.[28] Further, we consider a ring obtained from an InGaAs/InAlAs heterostructure[20] with $W=120$ nm for the width openings and $R_{\text{in}}=140$ nm and $R_{\text{out}}=265$ nm for the inner and outer radii, respectively. The effective mass of carriers is assumed to be $m=0.04m_0$, with m_0 the free electron mass. For the present case, we analyze an ideal ring without the presence of any defect. We adopt a tight-binding model to describe the Hamiltonian of the system.[29] The numerical technique is based on the calculation of the retarded Green's function of the system by using a recursive technique.[30–33] The method is quite general and allows to treat the possible influence of spin-orbit coupling on the system.[34] The presence of an external magnetic field can be modeled by adding Peierl's phases to the hopping elements of the Hamiltonian.[33]

We study the conductance variation of such an AB ring under the effect of a superimposed perturbing potential $U(x,y)$. In Figs. 2(a) and 2(d), we have first assumed a long-range Lorentzian function $U(r)=U_0/\{1+[r/\sigma]^2\}$, where $r=\sqrt{x^2+y^2}$, the coordinates x and y have the tip position as origin, U_0 is the maximum potential perturbation, and σ determines the decay rate of the potential. Notice that the spatial extension of such a potential is larger than 2σ. However, since recent experimental results on open quantum dots have pointed out that, in some cases, a significant spatial asymme-

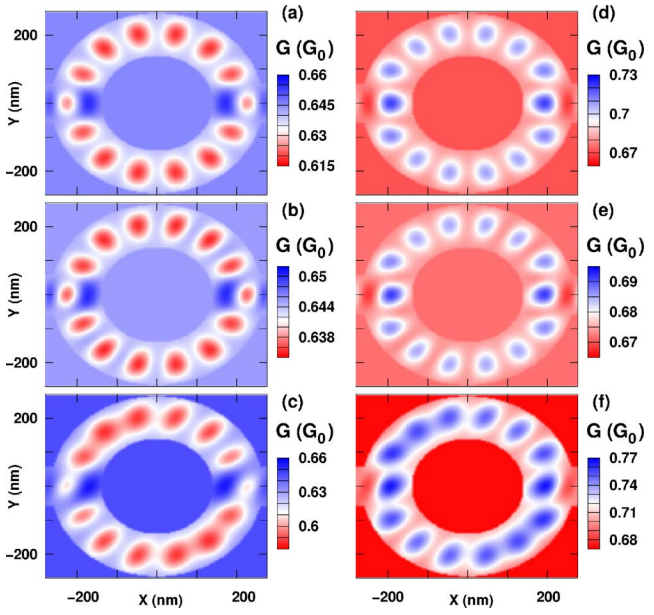

FIG. 2. (Color online) Conductance maps for an ideal AB ring with $W=120$ nm for the width openings and $R_{in}=140$ nm and $R_{out}=265$ nm for the inner and the outer radii, respectively. We have adopted a Fermi energy $\epsilon_F=1.65$ meV in (a)–(c) and $\epsilon_F=1.75$ meV in (d)–(f), whereas a maximum for the transmission energy stays at 1.7 meV. Therefore, figures on the left stay below and figures on the right stay above a resonance. For [(a) and (d)] the first-line couple, the perturbing potential mimicking the effect of the charged tip is modeled as $U(r)=U_0/\{1+[r/\sigma]^2\}$ with $U_0=\epsilon_F/10$ and $\sigma=10$ nm. For [(b) and (e)] the couple and [(c) and (f)] the couple, we have adopted the same asymmetric perturbing potential $U(r)=U_0/\{1+[(x+y)/\sigma]^2+[2(x-y)/\sigma]^2\}$ with $U_0=\epsilon_F/10$, but with different spatial extensions determined by $\sigma=10$ nm and $\sigma=40$ nm, respectively.

try characterizes the tip-induced potential,[35] we have also adopted an asymmetric shape for $U(x,y)$. In Figs. 2(b)–2(e) and in Figs. 2(c)–2(f), we have assumed the potential $U(x,y)=U_0/\{1+[(x+y)/\sigma]^2+[2(x-y)/\sigma]^2\}$ with $\sigma=10$ nm and $\sigma=40$ nm, respectively. Conductance maps on the left side of Fig. 2 have a Fermi energy slightly below a resonance for which the ring has maximal transmission $T=1$, whereas on the right side, they have a Fermi energy slightly above the resonance.

Since both energies are close each other, the mapped conductances are very similar and differ only for having opposite signs in complete agreement with Eq. (6). We notice that in order to properly model a realistic tip-induced potential a three-dimensional self-consistent solution of the Poisson–Schrödinger equation should be computed. Here, we want to emphasize that even if the correct shape of the perturbing potential should be obtained by computing the electrostatics of the total system, still the conductance variation does not depend on the particular shape of the potential in the linear-response regime under study.[21] A fully self-consistent calculation of the structure potential would be useful to determine the conditions on the tip parameters to work in this regime.

Concerning the effect of an asymmetric tip-induced potential, we observe that the small asymmetry in Figs. 2(b) and 2(e) can be considered negligible with respect to Figs. 2(a) and 2(d), obtained with a symmetric potential. On the contrary, it is relevant in Figs. 2(c) and 2(f) where the spatial extension of the perturbing potential becomes larger than $\lambda_F/2\sim 72$ nm giving rise to a nonlinear behavior of the conductance. We conclude that the effect of an asymmetric potential can be minimized by providing a tip-induced perturbation with limited spatial extension.

III. MULTICHANNEL TRANSMISSION

In this section, we extend the results obtained for the single-channel transmission to the case of the conductance being the sum of several channels as expressed by the Landauer–Büttiker formula $G=G_0\Sigma_n T_n$, where T_n is the transmission probability of the nth conducting transverse mode. This is the most common experimental situation.[20,21] In particular, we want to verify whenever the LDOS-ΔG correspondence depicted in Sec. II is valid for realistic 2D structures.

A first complication in obtaining a LDOS-ΔG correspondence arises from the spatial resolution of the scanning tip. Since the total wave function is given by the contribution of several transverse modes, each one with a different spatial periodicity, the LDOS presents usually a very complex shape, which would require a spatial resolution smaller than $\lambda_F/2$. Since this can be difficult to realize in real experiments, an inaccurate spatial resolution of the tip-induced perturbation would lead to properly take into account only conducting modes corresponding to the lowest energies and to lose a satisfactory correspondence with the LDOS. Another complication with respect to the single-channel case concerns the interpretation of conductance maps in terms of Hilbert transform of the LDOS. Generally, in the multichannel transmission case, it is not possible to obtain a direct LDOS-ΔG correspondence since the effect of the local perturbing potential is different for each transverse mode. In particular, we expect that the Hilbert transform of the LDOS acts as a filter selecting the states closest to the Fermi energy.

However, in mesoscopic structures such as open quantum dots[10] and AB rings,[21] it often occurs that the LDOS is dominated by the states closest to the Fermi level, which have a spatial periodicity quite larger than the half-Fermi wavelength. This allows us to soften the requirement on the tip resolution and to recover the LDOS-ΔG correspondence depicted in Sec. II because only one or few energetically close states determine the LDOS. In these specific cases, the same LDOS-ΔG correspondence for the one-channel case is recovered provided that the conditions found in Sec. II are valid. This means that the spatial extension of the tip-induced potential has to be smaller than the spatial periodicity of the dominant channels *and* the potential height U_0 has to be smaller than the corresponding energy levels.

In order to demonstrate the realization of such a situation, we discuss experimental SGM data from a quantum ring. The ring is fabricated from a InGaAs/InAlAs heterostructure using electron beam lithography and wet etching. The 2DEG is located 25 nm below the surface, and its low temperature electron density and mobility are 2×10^{16} m^{-2} and

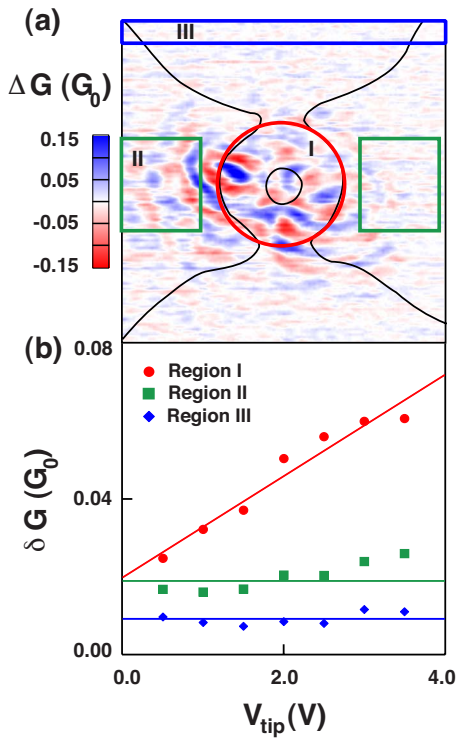

FIG. 3. (Color online) (a) Experimental conductance map measured for $V_{\mathrm{tip}}=2.5$ V and (b) averaged conductance variation δG as a function of the tip voltage V_{tip} measured in different device regions indicated in (a). A clear linear dependence is present only in region I inside the ring. The squared region in (a) has a side of 1.7 μm. The 2DEG distance of the tip is $D_{\mathrm{tip}}=50$ nm, $T=4.4$ K, and a magnetic field of $B=2$ T is applied perpendicularly to the surface.

10 $\mathrm{m}^2/\mathrm{V}\,\mathrm{s}$, respectively. The ring inner and outer (lithographic) radii are 120 and 290 nm (this sample is the same as sample R1 in Ref. 21). In Fig. 3(a), we show a conductance map measured on sample R1, with several modes transmitted through the ring's openings. The conductance map is characterized by radial conductance fringes with a spatial extension of about 100 nm, much larger than $\lambda_F/2$ (about 10 nm here). The large lateral extension of the fringes is most likely associated with resonant states close to the Fermi level dominating the LDOS.

We specify that such conductance images are obtained after subtraction of a tip-induced background from experimental data.[20,21] Such a background can be explained as follows. First of all, it is worth reminding the situation of a perfect conductor: The tip-sample interaction results in the formation of a superficial charge distribution fully determined by the capacitive coupling. This charge distribution corresponds to a perfect screening, so that an electron from the metallic gas sees a perfectly constant potential inside the sample layer. Hence, in such an ideal conductor, the impact of the tip is to change the concentration, but not to induce scattering. Now, in a real 2D sample, screening is not perfect, and the tip impact is twofold. On the one hand, there is still a change in electron concentration. This change is wide range and eminently depends on the tip shape (blunt or sharp). With a commercial tip, this results in a long-range modification of the electron concentration, which can also be seen as a change in the Fermi energy of the system. This is the reason for the background change of the conductance. On the other hand, screening is not perfect, and the electrons still see a screened potential, whose range is *effective* on a much smaller scale. This screened potential is responsible for the local electron wave scattering and provides the ability to deduce local parameters inside the nanostructure. The short-range character of this screened potential is demonstrated by the very existence of SGM data fluctuations occurring on a scale much shorter than what is indeed to be expected from an analysis relying only upon a charge modification. Hence, SGM data obtained with a tip position just above the active device part usually exhibit a background[10,20,21] because the conductance modification is due to the combination of both a long-range change in the Fermi energy (the so-called background) and of the local electron scattering induced by the unscreened, remaining part of the tip perturbation.

Consequently, in this work, we have chosen to simply model the tip-induced potential by means of a short-range potential responsible for the conductance variation, assuming that the effect of the long-range change of the Fermi energy does not bring information on LDOS properties and is included in the choice of ϵ_F.

From an experimental point of view, we demonstrate the feasibility of the linear-response regime in Fig. 3(b), where an averaged conductance variation as a function of the tip voltage is shown. Notice that a clear linear dependence on the tip voltage is experimentally found only if the tip scans region I inside the ring, where the former conditions are expected to hold.

In summary, specific situations exist such that the total wave function of the system adopts a simple and regular shape and the conditions for a satisfactory LDOS-ΔG correspondence are recovered. In the following, we give a few relevant examples on an AB ring and illustrate them with experimental data and numerical simulations.

A. Localized states in Aharonov–Bohm rings with impurities

We first focus on a realistic AB ring with the same size as the one studied in Sec. II, but with a random distribution of symmetry-breaking defects. These defects are probably responsible for the asymmetric conductance images in Ref. 21, where the wave function inside the ring is strongly influenced by localized states. In Fig. 4, we display a typical conductance map for the same ring as in Fig. 3. We notice that the conductance map inside the ring is characterized by radial asymmetric fringes in both Figs. 3(a) and 4.

Here, we model the defects by superimposing a randomly distributed analytical potential $V(r)$ to the structure profile. This takes into account the electrostatic effects of defects with charge Q at distance z from the 2DEG and reads

$$V(r)=\frac{Q}{4\pi\epsilon_0\epsilon_r z}\frac{I(a)}{1+aI(a)[(1+r^2/z^2)^{3/2}-1]}, \tag{9}$$

with $a=\frac{e^2mz}{2\pi\hbar^2\epsilon_0\epsilon_r}$ and $I(a)=\int_0^\infty \frac{xe^{-x}}{x+a}dx$.[36] In our simulations, we have adopted a random distribution with a 90 $\mu\mathrm{m}^{-2}$ numeri-

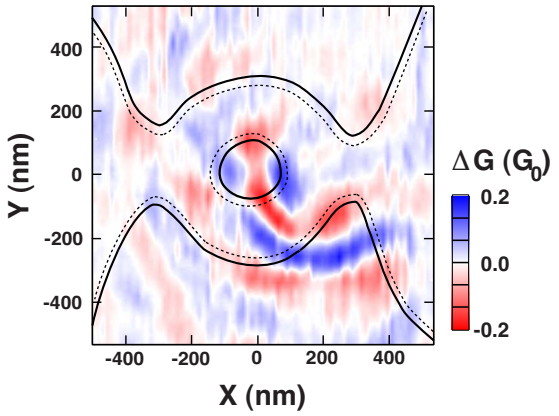

FIG. 4. (Color online) Experimental conductance map as a function of the tip position in the same sample as in Fig. 3. The dashed line indicates a depletion region at the border of the ring. $V_{\text{tip}}=0.5$ V, $D_{\text{tip}}=50$ nm, $T=4.2$ K, and $B=1.5$ T.

cal density at a fixed distance of 20 nm from the 2DEG. In Fig. 5, we show the impurity-induced potential profile used in our calculations.

Further, we have chosen a Fermi energy range for which more than ten conducting channels are present in the openings and more than 100 inside the ring.

The first favorable situation occurs when the LDOS is determined by the position of these defects. By computing the LDOS of the AB ring with the addition of randomly distributed impurities, we have found several images where the squared wave function of the system is dominated by such localized states.

As an example, Fig. 6 shows the LDOS of the AB ring with the presence of randomly distributed impurities for one of such specific energies, as well as the corresponding conductance variation due to a Lorentzian perturbing potential. In this case, the LDOS and the conductance variation are characterized by radial asymmetric fringes similar to those of Fig. 4. Even if the effective spatial extension of the tip-induced potential is larger than $\lambda_F/2\sim 9$ nm, the conductance map accurately reproduces the LDOS shape due to the large spatial extension of the localized states. We have also performed simulations with a repulsive impurity potential such as that created by negative-donor centers[37] and we have reached similar conclusions.

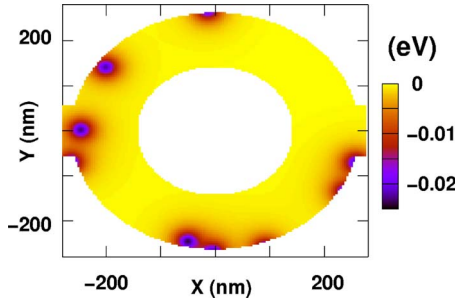

FIG. 5. (Color online) Potential profile due to randomly distributed impurities in a AB ring ($W=120$ nm, $R_{\text{in}}=140$ nm, and $R_{\text{out}}=265$ nm). These impurities are mainly localized around the border of the ring.

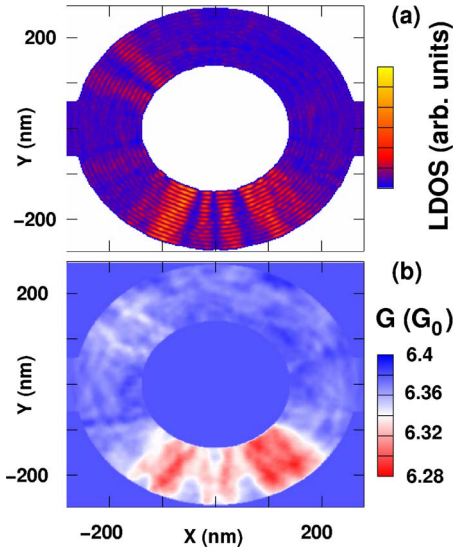

FIG. 6. (Color online) (a) LDOS and (b) conductance map of a realistic AB ring ($W=120$ nm, $R_{\text{in}}=140$ nm, and $R_{\text{out}}=265$ nm) with randomly distributed impurities. The presence of localized states is clearly visible in both of them. The perturbing potential mimicking the effect of the charged tip is modeled as the long-range potential $U(r)=U_0/\{1+[r/\sigma]^2\}$ with $U_0=\epsilon_F/100$ and $\sigma=5$ nm. Other parameters are $\epsilon_F=0.1074$ eV and $B=0$.

B. Semiclassical orbits in Aharonov–Bohm ring with impurities

Another favorable situation occurs in the presence of semiclassical orbits inside the mesoscopic structure.[38,39] They correspond to quasiclassical states that scar the total wave function of the system and recur periodically as the Fermi energy or an external magnetic field is varied.[38,39]

In Fig. 7, we plot the conductance of the AB ring with impurities as a function of the Fermi energy as well as its Fourier transform (inset). In the latter plot, it is possible to identify a sharp maximum at a frequency of 400 1/eV corresponding to the occurrence of a dominant pattern in the

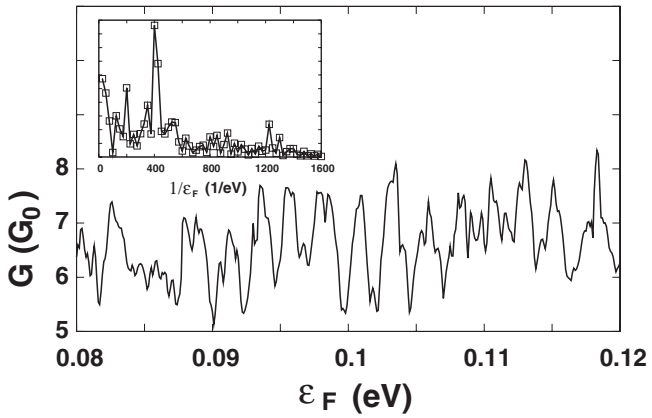

FIG. 7. Conductance as a function of the Fermi energy of the AB ring ($W=120$ nm, $R_{\text{in}}=140$ nm, and $R_{\text{out}}=265$ nm) with randomly distributed impurities. In the inset, the Fourier transform is plotted.

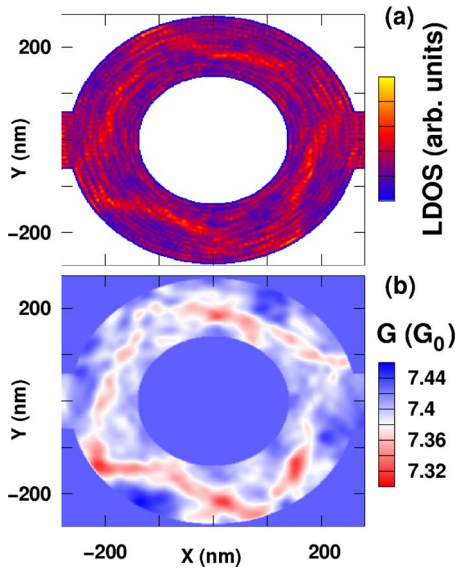

FIG. 8. (Color online) (a) LDOS and (b) conductance map of a realistic AB ring (W=120 nm, R_{in}=140 nm, and R_{out}=265 nm) with the presence of randomly distributed impurities. Semiclassical orbits are well visible in both maps. The perturbing potential mimicking the effect of the charged tip is modeled as a the long-range potential $U(r)=U_0/\{1+[r/\sigma]^2\}$, with ϵ_F=0.1008 eV, $U_0=\epsilon_F/50$, and σ=10 nm.

LDOS. Such a quasiclassical orbit is plotted in Fig. 8(a) and was found to recur with a frequency of 400 1/eV. Also, in this case, the large and uniform spatial extension of the wave function permits to recover a clear correspondence with the conductance map shown in Fig. 8(b).

Finally, we notice that these results do not depend on the particular potential profile of the investigated device. We expect that a nice LDOS-ΔG correspondence can be recovered in any structure presenting a LDOS dominated by conducting modes reacting in a similar way to the effect of the scanning tip. In particular, the LDOS of structures such as open quantum dots exhibiting signatures of scarred wave functions[10] can be reliably probed with the SGM technique, provided that the above-mentioned conditions on the amplitude and lateral extension of the perturbing potential are met.

IV. CONCLUSION

We have presented a theoretical analysis of scanning gate microscopy as an experimental tool to image the LDOS of mesoscopic samples fabricated from buried 2D electron systems such as Aharonov–Bohm rings.

We have shown that in the single-channel transmission case a generalized Kramers–Kronig relation holds between the LDOS of the system and the conductance variation due to the scanning tip. Such a relationship is valid in the linear-response regime where the tip induced potential is so weak that the energy levels of the system are unchanged. In this case, we have shown a striking correspondence between LDOS and ΔG images for a symmetric double-barrier system and an AB ring.

In the multichannel transmission case, an exact LDOS-ΔG correspondence is less straightforward due to the deficient spatial resolution of the tip-induced potential and to the uneven effect of the tip on the different transverse modes. However, in some special cases for which the total wave function is determined only by the states closest to the Fermi energy and presents a large and uniform spatial extension, such a correspondence can be still recovered. In particular, we have shown a nice agreement between LDOS and conductance images when the LDOS is dominated by localized states or by semiclassical periodic orbits responsible for wave function scarring effects.

ACKNOWLEDGMENTS

We would like to thank M. Governale, M. Büttiker, and D. K. Ferry for useful discussions and suggestions. This work is supported by the *PNANO 2007* program of the *Agence Nationale de la Recherche* ("MICATEC" project). B.H. acknowledges funding by the FNRS (Belgium) and by the Belgian Science Policy (Interuniversity Attraction Pole Program IAP).

[1] M. F. Crommie, C. P. Lutz, and D. M. Eigler, Science **262**, 218 (1993).
[2] M. A. Topinka, B. J. LeRoy, S. E. J. Shaw, E. J. Heller, R. M. Westervelt, K. D. Maranowski, and A. C. Gossard, Science **289**, 2323 (2000).
[3] M. A. Topinka, B. J. LeRoy, R. M. Westervelt, S. E. J. Shaw, R. Fleischmann, E. J. Heller, K. D. Maranowski, and A. C. Gossard, Nature (London) **410**, 183 (2001).
[4] N. Aoki, C. R. Da Cunha, R. Akis, D. K. Ferry, and Y. Ochiai, Appl. Phys. Lett. **87**, 223501 (2005).
[5] C. R. da Cunha, N. Aoki, T. Morimoto, Y. Ochiai, R. Akis, and D. K. Ferry, Appl. Phys. Lett. **89**, 242109 (2006).
[6] M. P. Jura, M. A. Topinka, L. Urban, A. Yazdani, H. Shtrikman, L. N. Pfeiffer, K. W. West, and D. Goldhaber-Gordon, Nat. Phys. **3**, 841 (2007).
[7] A. Pioda, S. Kicin, T. Ihn, M. Sigrist, A. Fuhrer, K. Ensslin, A. Weichselbaum, S. E. Ulloa, M. Reinwald, and W. Wegscheider, Phys. Rev. Lett. **93**, 216801 (2004).
[8] P. Fallahi, A. C. Bleszynski, R. M. Westervelt, J. Huang, J. D. Walls, E. J. Heller, M. Hanson, and A. C. Gossard, Nano Lett. **5**, 223 (2005).
[9] A. Bachtold, M. S. Fuhrer, S. Plyasunov, M. Forero, E. H. Anderson, A. Zettl, and P. L. McEuen, Phys. Rev. Lett. **84**, 6082 (2000).
[10] R. Crook, C. G. Smith, A. C. Graham, I. Farrer, H. E. Beere, and D. A. Ritchie, Phys. Rev. Lett. **91**, 246803 (2003).
[11] G. Finkelstein, P. I. Glicofridis, R. C. Ashoori, and M. Shayegan, Science **289**, 90 (2000).

[12] N. Aoki, C. R. da Cunha, R. Akis, D. K. Ferry, and Y. Ochiai, Phys. Rev. B **72**, 155327 (2005).
[13] A. Baumgartner, T. Ihn, K. Ensslin, K. Maranowski, and A. C. Gossard, Phys. Rev. B **76**, 085316 (2007).
[14] J. Weis, Int. J. Mod. Phys. B **21**, 1297 (2007).
[15] A. C. Bleszynski, F. A. Zwanenburg, R. M. Westervelt, A. L. Roest, E. P. A. M. Bakkers, and L. P. Kouwenhoven, Nano Lett. **7**, 2559 (2007).
[16] M. Mendoza and P. A. Schulz, Phys. Rev. B **68**, 205302 (2003).
[17] M. Mendoza and P. A. Schulz, Phys. Rev. B **71**, 245303 (2005).
[18] G. Metalidis and P. Bruno, Phys. Rev. B **72**, 235304 (2005).
[19] A. Cresti, J. Appl. Phys. **100**, 053711 (2006).
[20] B. Hackens, F. Martins, T. Ouisse, H. Sellier, S. Bollaert, X. Wallart, A. Cappy, J. Chevrier, V. Bayot, and S. Huant, Nat. Phys. **2**, 826 (2006).
[21] F. Martins, B. Hackens, M. G. Pala, T. Ouisse, H. Sellier, X. Wallart, S. Bollaert, A. Cappy, J. Chevrier, V. Bayot, and S. Huant, Phys. Rev. Lett. **99**, 136807 (2007).
[22] R. Landauer, IBM J. Res. Dev. **1**, 233 (1957); M. Büttiker, Phys. Rev. Lett. **57**, 1761 (1986).
[23] B. Hackens, S. Faniel, C. Gustin, X. Wallart, S. Bollaert, A. Cappy, and V. Bayot, Phys. Rev. Lett. **94**, 146802 (2005).
[24] S. Datta, *Electronic Transport in Mesoscopic Systems* (Cambridge University Press, Cambridge, 1995).
[25] G. D. Mahan, *Many-Particle Physics* (Plenum, New York, 1981).
[26] F. Sols, M. Macucci, U. Ravaioli, and K. Hess, J. Appl. Phys. **66**, 3892 (1989).
[27] V. Gasparian, T. Christen, and M. Büttiker, Phys. Rev. A **54**, 4022 (1996).
[28] M. G. Pala and G. Iannaccone, Phys. Rev. B **69**, 235304 (2004).
[29] F. Mireles and G. Kirczenow, Phys. Rev. B **64**, 024426 (2001).
[30] H. U. Baranger, D. P. Di Vincenzo, R. A. Jalabert, and A. D. Stone, Phys. Rev. B **44**, 10637 (1991).
[31] D. K. Ferry and S. M. Goodnick, *Transport in Nanostructures* (Cambridge University Press, Cambridge, UK, 1997).
[32] D. Frustaglia, M. Hentschel, and K. Richter, Phys. Rev. Lett. **87**, 256602 (2001).
[33] M. G. Pala, M. Governale, U. Zülicke, and G. Iannaccone, Phys. Rev. B **71**, 115306 (2005).
[34] Th. Schäpers, V. A. Guzenko, M. G. Pala, U. Zülicke, M. Governale, J. Knobbe, and H. Hardtdegen, Phys. Rev. B **74**, 081301(R) (2006).
[35] A. E. Gildemeister, T. Ihn, M. Sigrist, K. Ensslin, D. C. Driscoll, and A. C. Gossard, Phys. Rev. B **75**, 195338 (2007).
[36] F. Stern and W. E. Howard, Phys. Rev. **163**, 816 (1967).
[37] S. Huant, A. Mandray, G. Martinez, M. Grynberg, and B. Etienne, Surf. Sci. **263**, 565 (1992).
[38] R. Akis, D. K. Ferry, and J. P. Bird, Phys. Rev. Lett. **79**, 123 (1997).
[39] J. P. Bird, R. Akis, D. K. Ferry, D. Vasileska, J. Cooper, Y. Aoyagi, and T. Sugano, Phys. Rev. Lett. **82**, 4691 (1999).